ACS APPLIED MATERIALS & INTERFACES

Research Article

www.acsami.org

Extraordinary Reinforcement Effect of Three-Dimensionally Nanoporous Cellulose Gels in Poly(ε-caprolactone) Bionanocomposites

Kai Li,[†] Jianhui Song,[‡] Min Xu,[‡] Shigenori Kuga,[§] Lina Zhang,[†] and Jie Cai*,[†]

[†]College of Chemistry & Molecular Sciences, Wuhan University, Wuhan 430072, People's Republic of China

[‡]Department of Physics, Shanghai Key Laboratory of Magnetic Resonance, East China Normal University, Shanghai 200062, People's Republic of China

[§]Graduate School of Agricultural and Life Sciences, The University of Tokyo, Tokyo, Japan

Supporting Information

ABSTRACT: Three-dimensionally nanoporous cellulose gels (NCG) were prepared by dissolution and coagulation of cellulose from aqueous alkali hydroxide-urea solution, and used to fabricate NCG/poly(ε-caprolactone) (PCL) nanocomposites by in situ ring-opening polymerization of ε-CL monomer in the NCG. The NCG content of the NCG/PCL nanocomposite could be controlled between 7 and 38% v/v by changing water content of starting hydrogel by compression dewatering. FT-IR and solid-state ^{13}C NMR showed that the grafting of PCL onto cellulose are most likely occurred at the C6-OH groups and the grafting percentage of PCL is 25 wt % for the nanocomposite with 7% v/v NCG. ^{1}H NMR, XRD, and DSC results indicate that the number-average molecular weight and crystal formation of PCL in the nanocomposites are remarkably restricted by the presence of NCG. AFM images confirm that the interconnected nanofibrillar cellulose network structure of NCG are finely distributed and preserved well in the PCL matrix after polymerization. DMA results show remarkable increase in tensile storage modulus of the nanocomposites above glass transition and melting temperatures of the PCL matrix. The percolation model was used to evaluate the mechanical properties of the nanocomposites, in which stress transfer among the interconnected nanofibrillar network is facilitated through strong intermolecular hydrogen bonding and entanglement of cellulose nanofibers.

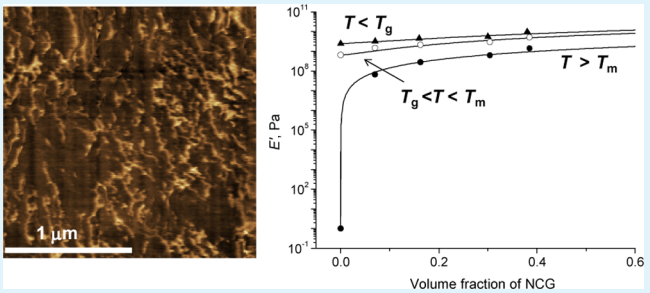

KEYWORDS: *nanoporous cellulose gel, poly(ε-caprolactone), bionanocomposites, percolation model, mechanical properties*

INTRODUCTION

Bionanocomposites formed by combination of biopolymer matrix and nanofillers having led to a rapidly increasing interest due to the environmental awareness and demand for green technology.[1,2] Poly(ε-caprolactone) (PCL) is a hydrophobic, semi-crystalline, and degradable polyester. It has been used in packing, tissue engineering, and biomedical applications, but is also hampered by their poor mechanical strength.[3]

The rigid nanofillers, such as carbon nanotubes,[4,5] cellulose nanofibers/nanowhiskers,[6−14] clay,[15,16] graphene,[5,17,18] and self-assembled carbon nanotube and graphene,[19,20] cellulose nanofibers/nanowhiskers gels,[21−26] and bacteria cellulose gels[27−29] have been used to prepare nanocomposites, which exhibit remarkable properties such as electric conduction, high mechanical strengths, thermal stability, and gas-barrier properties.

Among these nanofillers, cellulose nanofibers/nanowhiskers derived from cotton, wood, or tunicate attract special attention because of their remarkable physical properties, such as low density, high specific surface area, high elastic modulus, low thermal expansivity, and chiral nematic ordering capability of aqueous suspension.[10,11,30−33] Practical utilization of hydrophilic cellulose nanofibrials/nanowhiskers for polymer composites, however, is still a challenge with regard to production cost and difficulty inhomogeneous dispersion in hydrophobic matrices.[25,30,32,34] Many attempts to prepare cellulose nanofibers/nanowhisker-based polymer nanocomposites include surface functionalization by covalently bound groups, surfactant adsorption,[6,7,13,34−45] use of self-assembled templates from aqueous suspension,[22−25] and supercritical drying.[26]

Although the majority of reported works deal with nanofiber/nanowhisker with native (cellulose I) crystallinity, cellulose can be prepared as hydrogel with regenerated (cellulose II) crystallinity via dissolution and coagulation. Recently, we found that aqueous alkali hydroxide-urea solution is particularly suited for gel preparation. The resulting three-dimensionally nanoporous cellulose gel (NCG) has been shown to give remarkable mechanical strength, high light

Received: January 16, 2014
Accepted: April 29, 2014
Published: April 29, 2014

Table 1. Physical Properties of the Neat PCL, NCG, and NCG/PCL Nanocomposites

sample	NCG (v/v%)	PCL (w/w%)	M_n[a] (g/mol)	ΔH_m, J/g	χ_c (%) DSC[b]	χ_c (%) XRD[c]	D (nm)	T_m (°C)	σ_b (MPa)	ε_b (%)	E (MPa)
PCL	0	100	23 400	71.7	46	77	39.9	57.5	9.8	691	175
NCG/PCL-1	7	90	6500	46.4	32	60	11.6	54.3	17.7	9	429
NCG/PCL-2	16	78	3500	28.4	22	56	12.4	52.4	18.5	13	535
NCG/PCL-3	30	62	3100	20.4	19	51	9.7	50.4	21.6	9	654
NCG/PCL-4	38	53	2800	10.0	10	53	7.0	46.3	25.8	11	775

[a] M_n, number-average molecular weight of the PCL; [b] χ_c, crystallinity of the PCL, determined by DSC; [c] χ_c, crystallinity of the neat PCL and NCG/PCL nanocomposites, determined by XRD; σ_b, ε_b and E are the tensile strength, elongation at break, and Young's modulus of the PCL and nanocomposites.

transmittance, and porosity of nanometer orders.[46] NCG's usefulness as nanomaterial has been demonstrated through aerogel preparation,[47] and in situ synthesis of metallic, inorganic, and conductive nanoparticles.[48−50] It can also serve as substrate of tough, foldable, and transparent composite films.[51] The aim of the present work is to develop a strategy for the NCG/PCL nanocomposites via in-situ ring-opening polymerization of ε-caprolactone (ε-CL), and to study the mechanical reinforcement effects of the NCG in the PCL matrix.

EXPERIMENTAL SECTION

Materials. ε-Caprolactone (ε-CL) was dried over CaH_2, distilled under reduced pressure. Acetone, chloroform, tetrahydrofuran (THF), tin octoate ($SnOct_2$), dodecanol, lithium hydroxide hydrate, and urea were used as received. Cellulose (cotton linter pulp) with viscosity-average molecular weight (M_η) of 9.2×10^4 was provided by Sanyou Chemical Fiber Co. Ltd. (Tangshan, China), and dried in vacuum at 60 °C for 24 h prior to use.

Fabrication of NCG Hydrogels. Cellulose was dissolved in an aqueous 4.6 wt % LiOH/15 wt % urea solution pre-cooled to −12 °C to form a 6 wt % transparent cellulose solution according to our previous method.[46] The cellulose solution was subjected to centrifugation to remove air bubbles, spread on a glass plate and coagulated by ethanol to form gel, which was thoroughly washed with deionized water. Thickness of the gel was made 1, 3, 4, and 6 mm.

Fabrication of NCG Film. The NCG hydrogel with 1 mm thickness was fixed on a plastic plate at ambient temperature, to evaporate the water and dry the resulting film, which had a thickness of ca. 0.1 mm.

Fabrication of NCG/PCL Nanocomposites in NCG by in Situ Ring-Opening Polymerization. The hydrogels were compressed under 0.2 MPa at 60 °C to ca. 1 mm to form hydrogels with different water content, i.e., varied porosity. The NCG hydrogels were subjected to solvent-exchange to acetone, then to chloroform, and immersed at ambient temperature in neat ε-CL containing 1.8 wt % $Sn(Oct)_2$ as catalyst and 0.16 wt % dodecanol as initiator for 12 h. The gel was then placed in an ampoule connected to a Schlenk line, sealed with a Teflon septum and degassed by three vacuum/N_2 cycles. This procedure was effective to remove chloroform (bp 61.2°C) from ε-CL (bp 253°C). Polymerization was allowed to proceed at 120 °C for 12 h. Reference sample of neat PCL was prepared using the same procedure. The volume fraction of NCG in the nanocomposite was determined gravimetrically as an average of at least 3 independently prepared samples. The densities of cellulose and PCL are 1.62 and 1.2 g/cm^3, respectively.[49,52] The composition of nanocomposites is listed in Table 1.

Characterizations. *Fourier Transform Infrared (FT-IR) Spectroscopy.* FT-IR spectra were recorded at ambient temperature on a FT-IR spectrometer (Nicolet 5700 FTIR Spectrometer, MA) in the wavelength range from 4000 to 400 cm^{-1} with a 2 cm^{-1} resolution and an accumulation of 32 scans.

Wide-Angle X-ray Diffraction (WAXD). WAXD measurements were carried out on a WAXD diffractometer (D8-Advance, Bruker, USA) in reflection mode. The X-ray used was Ni-filtered CuK_α radiation with a wavelength of 1.5418 Å. The voltage was set at 40 kV and the current was set at 40 mA. Measurement was done by 2θ = 2° min^{-1} scan over 2θ range of 8 to 40°. The peak position and crystallinity of the nanocomposites was determined by multi-peak fitting of the XRD profiles, and apparent crystallite size (D) was estimated by Scherrer's formula

$$D = \frac{0.9\lambda}{\beta \cos\theta} \tag{1}$$

with

$$\beta = \sqrt{B^2 - b^2} \tag{2}$$

where λ is the wavelength of the CuK_α line; b is the instrumental constant (0.1°); B is the full-width half maximum in radian of diffraction peak; and 2θ is the peak angle in radian.

Nuclear Magnetic Resonance (NMR). The nanocomposites were washed with THF for 24 h using Soxhlet extraction to remove the free PCL within the NCG. ^{1}H NMR spectra of the extracted free PCL were recorded at 300 MHz on a Bruker AMX300 using $CDCl_3$ as solvent. The conversion of the ε-CL monomer was calculated from ^{1}H NMR signals at 4.05 (−CH_2O−, PCL repeating unit) and 4.20 (−CH_2O−, ε-CL). The number-average molecular weight (M_n) of the free PCL was also estimated with ^{1}H NMR using signals at 4.05 (−CH_2O−, PCL repeating unit) and 3.62 (−CH_2OH, PCL end group).[53] Solid-state ^{13}C NMR [cross/polarization, magic/angle spinning and dipolar decoupling (CP/MAS/DD)] measurements were carried out on a Bruker AVANCE/III spectrometer operating at 75.47 MHz at room temperature. The contact time for cross/polarization was 3 ms, the spin rate of the 4 mm rotor was 5 kHz. The ratio of the number of ε-CL monomer to anhydroglucose unit of cellulose was determined by quantitative cross-polarization (QCP) in solid-state NMR. The QCP scheme is based on reciprocity relation between cross-polarization (CP) and cross depolarization (CDP).[54,55] For each sample, one CP/MAS NMR spectra with certain polarization time and two CDP/MAS NMR spectra with different depolarization time were performed. The spin rate of the 4 mm rotor was 9 kHz.

Atomic Force Microscopy (AFM). The nanocomposite was cryo-microtomed at −30 °C to obtain smooth surfaces by an Ultracut FC4E (Reichert-Jung). The surface and cross-section of the sample were examined by a SPM-9500J3 multi-mode SPM (Shimadzu, Japan).

Differential Scanning Calorimetry (DSC). DSC was performed using a DSC Q20 differential scanning calorimeter (TA Instruments, USA) to evaluate the crystallinity (χ_c) and melting points (T_m) of the PCL in nanocomposites. Around 15 mg of sample was placed in a DSC cell. Each sample was heated from −80 to 100°C at 10°C/min, kept at 100 °C for 2 min, and then cooled down at same rate. The χ_c of the PCL was calculated from the melting transition as follows[56]

$$\chi_c = \frac{\Delta H_m}{w \Delta H_m^\circ} \tag{3}$$

where ΔH_m is the heat of fusion of the sample, ΔH_m° (157 J/g) is the heat of fusion for 100% crystalline PCL, and w is the weight fraction of PCL in the nanocomposites.

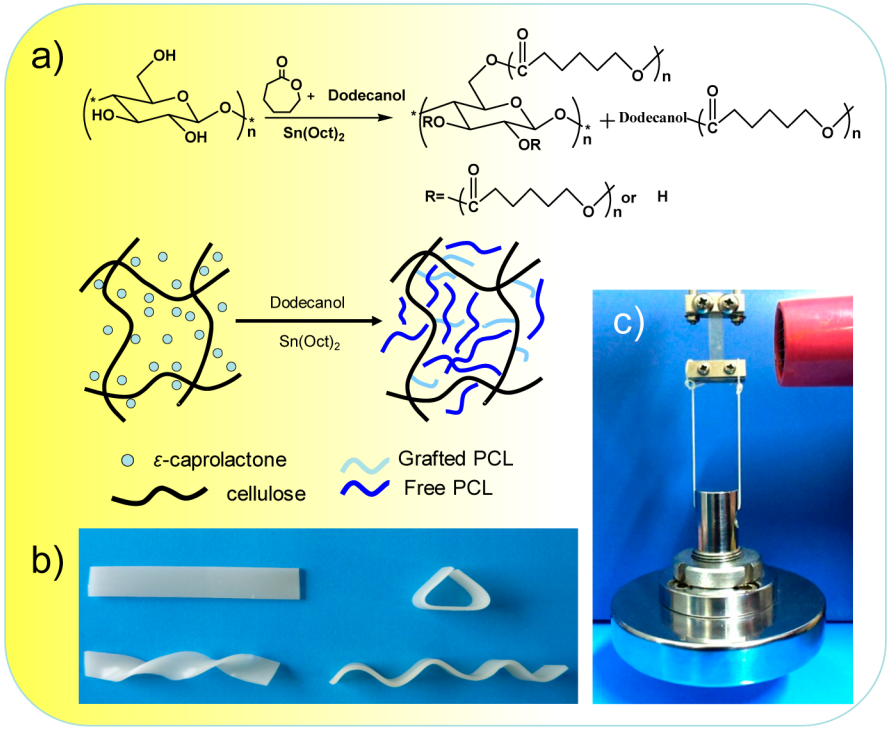

Figure 1. (a) Scheme of in situ ring-opening polymerization of ε-CL in NCG, (b) photographs of the reshaped NCG/PCL nanocomposite sheets, and (c) a weight of 1500 g in weight clung onto the down side of a NCG/PCL nanocomposite sheet (50 mm × 4.3 mm × 0.8 mm) containing 16% v/v NCG under heating flow.

Dynamic Mechanical Analysis (DMA). DMA temperature sweeps under oscillatory stress were performed on the nanocomposites using a DMA Q800 (TA Instruments, USA) in tensile mode at a heating rate of 5 °C/min and a distance between jaws of 10 mm in the temperature range from −100 to 150 °C with a frequency of 1 Hz. The width of the samples was about 5 mm.

Thermogravimetry Analysis (TGA). TGA analysis for the nanocomposites were performed on a STA 449C thermal analyzer (NETZSCH, Germany) under nitrogen at a heating rate of 10°C/min from 30 to 600°C.

Contact Angle Testing. Contact angle was measured by a Contact Angle System OCA20 (Germany). A drop of water (ca. 5 μL) was put on the sample and droplet shape was recorded over a period of 60 s.

Tensile Test. Stress-strain experiments were performed on a universal tensile tester (CMT 6503, SANS Test machine Co. Ltd., China) at 5 mm/min stretch, with 30 mm span at 25°C.

RESULTS AND DISCUSSION

The NCG hydrogels can provide large pore volume for polymerization of ε-CL, with abundant hydroxyl groups acting as initiator (Figure 1a). High conversion of 96% to 100% monomer to polymer was observed in all trials. Because of the thermoplasticity of PCL, the nanocomposites can be reshaped by heating (Figure 1b). Moreover, the opaque NCG/PCL nanocomposite containing 16% v/v NCG became transparent under heating flow and showed hardly deformation under a tension force of 445 N/cm^2 for a long time, demonstrating excellent mechanical stability of the nanocomposites above the melting temperature of the PCL matrix (Figure 1c and Movie S1 in the Supporting Information).

The FT-IR spectra of nanocomposites are superposition of those of cellulose and PCL (Figure 2). The strong peak from carboxyl stretching at 1726 cm^{-1} indicates the presence of PCL. Also, the peaks located around 1636 to 1620 cm^{-1} and 1730 to 1720 cm^{-1} overlapped with the neat PCL were probably for

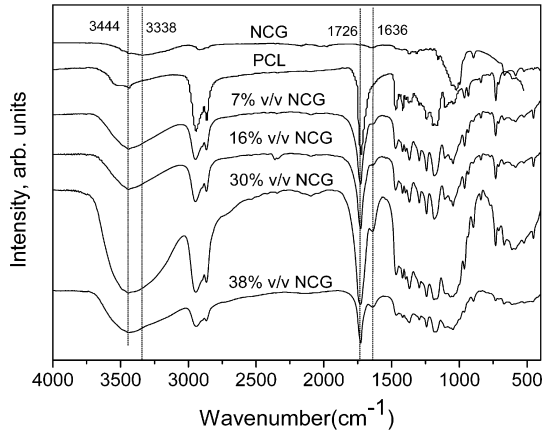

Figure 2. FT-IR spectra of the NCG, PCL, and NCG/PCL nanocomposites.

PCL-*g*-NCG,[26,56] which cannot be removed through Soxhlet extraction (not shown). The C−H stretching peaks (2800 to 3000 cm^{-1}) become prominent by increased PCL content in comparison to O−H stretching peak of cellulose (3000 to 3600 cm^{-1}). The shift of this peak from 3338 to 3444 cm^{-1} is likely to result from enhanced of hydrogen bonding between cellulose hydroxyls and the ester groups of PCL.

The CP/MAS ^{13}C NMR spectra of the NCG/PCL nanocomposites show synthesis of characteristic peaks of cellulose ($C_{1'}$, 107.4 and 105.3 ppm; $C_{2'}$, 73.4 ppm; $C_{3'}$, 77.0 ppm; $C_{4'}$, 89.2 and 88.0 ppm; $C_{5'}$, 75.2 ppm; $C_{6'}$, 63.1 ppm) and PCL (C_1, 174.6 ppm; C_2, 66.5 ppm; C_3, 30.2 ppm; $C_{4,5}$, 26.7 ppm; C_6, 34.3 ppm) (Figure 3).[57,58] A new peak at around 55 ppm emerged in the nanocomposites after Soxhlet extraction with THF, not belonging to either neat PCL or

dx.doi.org/10.1021/am500337p | ACS Appl. Mater. Interfaces 2014, 6, 7204−7213

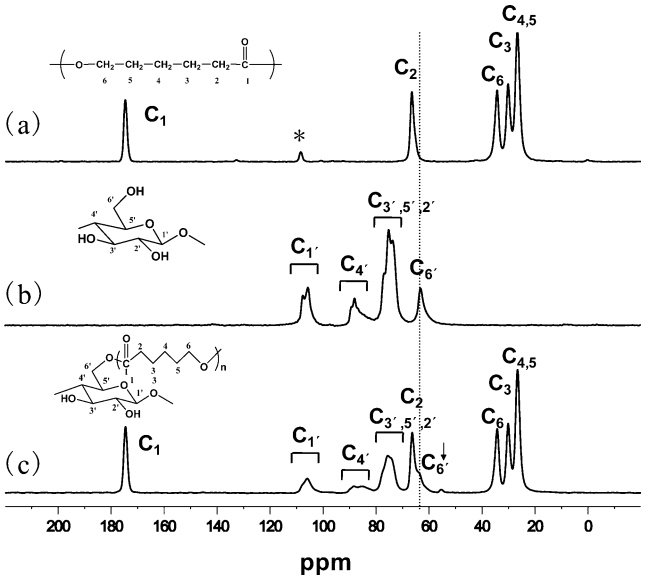

Figure 3. Solid-state CP/MAS ^{13}C NMR of the (a) PCL, (b) NCG, and (c) NCG/PCL nanocomposite after Soxhlet extracting with THF.

cellulose. This peak can be attributed to the C6 of cellulose at grafting point. This feature is consistent with a previous study that showed the derivatization of cellulose most likely occurred at the C6-OH groups because of steric advantage.[59]

QCP was used to evaluate the graft ratio of NCG/PCL nanocomposite (Figure 4). The signals of C═O of PCL and C-1 of NCG were selected to calculate for their good resolution. For a certain group, one can get the enhancement factor (η) of CP based on the reciprocity relation

$$\eta = [1 - \mathrm{CDP}_{(\text{long time})}/\mathrm{CDP}_{(\text{short time})}](\gamma_H/\gamma_C) \quad (4)$$

where $CDP_{(\text{long time})}$ and $CDP_{(\text{short time})}$ were peak intensity of two CDP/MAS NMR spectra with different depolarization time, γ_H/γ_C is equal to 3.98. Combined the corresponding CP/MAS NMR spectra, the weighted peak intensity (WPI) of the certain CP signal can be represented by

$$\mathrm{WPI} = \mathrm{PI}/\eta \quad (5)$$

where PI is the peak intensity of the certain group in CP experiment.

Despite not being able to establish the average degree of polymerization of the grafted PCL, the ratio of the number of ε-CL monomer to anhydroglucose unit of cellulose were evaluated from QCP NMR and listed in Table 2. The C═O/C-1 values of the NCG/PCL nanocomposite with 7% v/v NCG before and after Soxhlet extracting are 7.3 and 2.2, respectively. Based on these values, the grafting percentage of the PCL can be calculated to be 25 wt %. The M_n of the free PCL in the nanocomposites decreased when NCG content increased (Table 1). This behavior can be attributed to the increase of hydroxyl groups of cellulose serving as initiating site.

Table 2. Results from QCP NMR of the NCG/PCL Nanocomposite with 7% v/v NCG before and after Soxhlet Extracting with THF (Denoted as NCG/PCL-1a and NCG/PCL-1b, Respectively)

samples	η(C═O of PCL)	η(C-1 of cellulose)	C═O/C-1
NCG/PCL-1a	1.61	2.67	7.3
NCG/PCL-1b	1.82	2.65	2.2

Figure 5 shows the XRD patterns of the neat PCL, NCG and NCG/PCL nanocomposites. The patterns are nearly systematic superposition of those of neat PCL and NCG. Based on multi-peak fitting and estimation with the Scherrer equation, the crystallinity of the nanocomposites and crystallite size of the PCL were calculated and are listed in Table 1. Remarkably, the crystallinity of the nanocomposites decreases from 77% of neat PCL to 53% for the nanocomposite with 38% v/v NCG. The crystallite sizes estimated by the Scherrer equation were 39.9 nm for the neat PCL and decreased to 7.0−11.6 nm for the PCL in the nanocomposites. These features demonstrate that

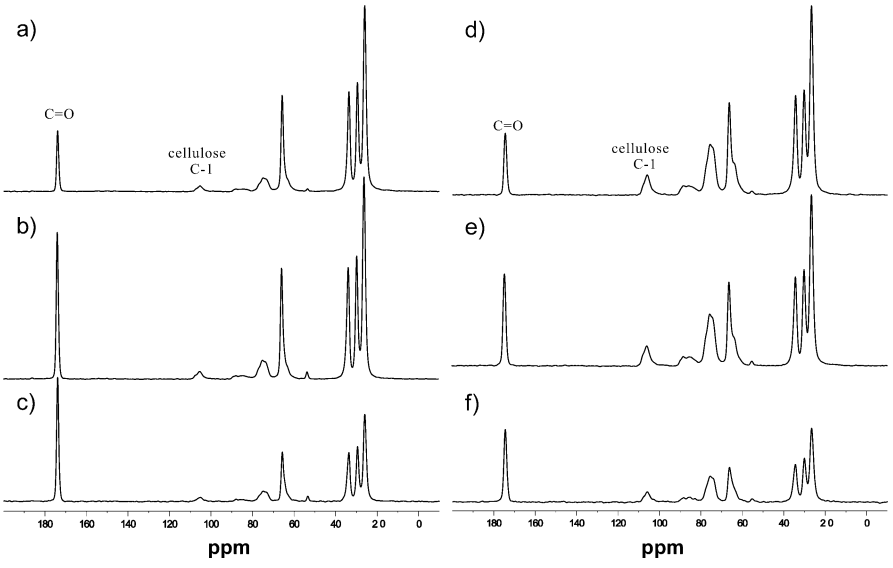

Figure 4. Left: (a) CP/MAS and (b, c) CDP/MAS ^{13}C NMR spectra of the NCG/PCL nanocomposite containing 7% v/v NCG. (a) 0.2 ms polarization time; (b) 0.001 ms depolarization time; (c) 0.2 ms depolarization time. Right: (d) CP/MAS and (e, f) CDP/MAS ^{13}CNMR spectra of the NCG/PCL nanocomposite (7% v/v NCG) after Soxhlet extracting with THF. (d) 0.3 ms polarization time; (e) 0.001 ms depolarization time; (f) 0.3 ms depolarization time.

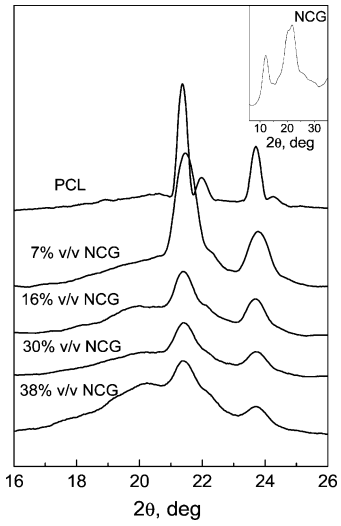

Figure 5. XRD patterns of the PCL, NCG, and NCG/PCL nanocomposites.

the crystallization of the PCL was severely restricted by the interconnected nanofibrillar cellulose network of the NCG.

The DSC thermograms of the neat PCL and nanocomposites are shown in Figure 6. The melting temperature (T_m), heat of

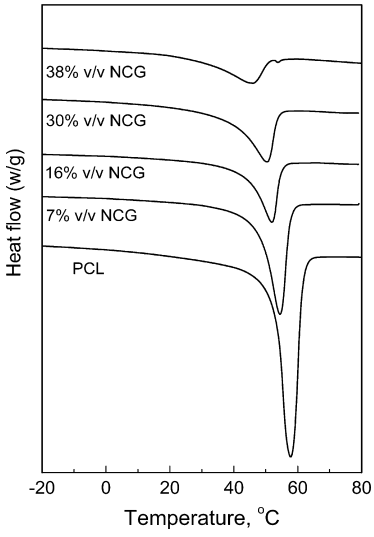

Figure 6. DSC thermogram of the PCL and NCG/PCL nanocomposites.

fusion (ΔH_m) and crystallinity (χ_c) of the PCL in nanocomposites were established by DSC and are summarized in Table 1. While the neat PCL shows typical melting endotherm with T_m of 58°C, those in nanocomposites are diminished and shifted to lower temperature with increasing NCG content. For instance, the NCG/PCL nanocomposite containing 38% v/v NCG showed the lowest T_m of 46.3°C and a crystallinity of 10% for the PCL matrix. All these changes are result of restricted crystallization and smaller molecular weight of PCL in the nanocomposites.

The nanocomposites showed remarkably improved water resistance over the NCG. Swelling by deionized water after 24 h immersion was nearly proportional to NCG content of the nanocomposites (Figure 7), an inevitable feature because of hydrophilicity of cellulose. The water contact angle of the NCG

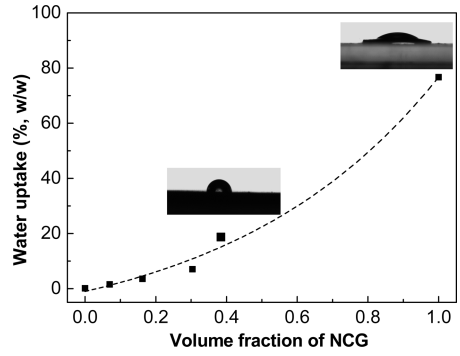

Figure 7. Water uptake as a function of NCG content for 24 h immersion. Inserted photographs of a water droplet deposited on the surface of NCG (upper right) and NCG/PCL nanocomposite containing 38% v/v NCG (bottom left).

film was 43°, and decreased rapidly because of the absorption by cellulose. Expectably, hybridization with PCL made the nanocomposites more hydrophobic.

Microscopic morphology and structure were examined by AFM by tapping-mode (Figure 8). The topography images and

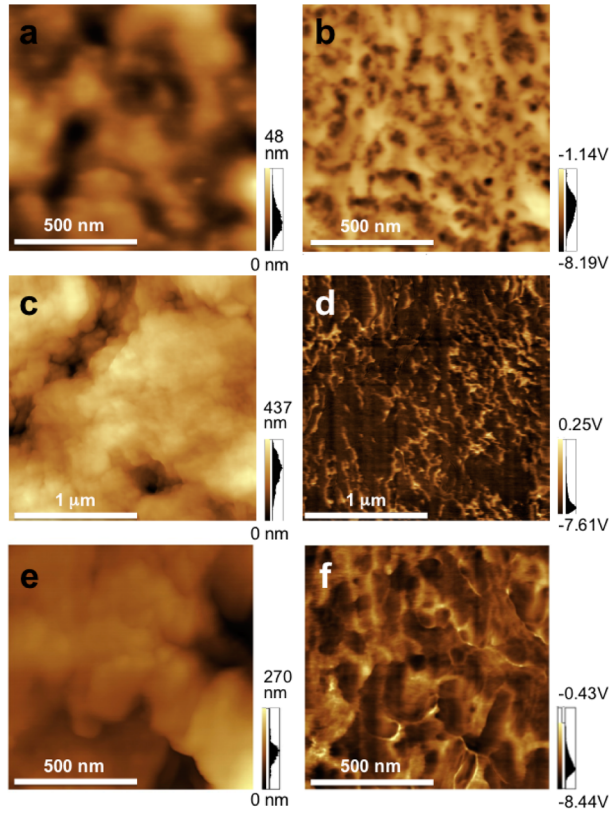

Figure 8. AFM topography images (left) and phase contrast images (right) of the nanocomposites containing 7% v/v NCG: (a, b) the surface, (c, d) cryo-microtomed inner part at low magnification, and (e, f) high-resolution images of the nanocomposite.

phase contrast images on the surface of the nanocomposite revealed uniform morphology with emerging of the NCG in PCL matrix (Figure 8a, b). The image of the cryo-fractured specimen (Figure 8d) reveals a homogenous distribution of nanofibrillar cellulose network similar to that of neat NCG. The observation at higher resolution (Figure 8e, f) confirmed again that interconnected cellulose nanofibers embedded in PCL

matrix. Overall, the images support that the interconnected nanofibrillar network structure of NCG is preserved well and finely distributed in nanocomposites after in situ polymerization.

Figure 9 shows dynamic mechanical behavior of the nanocomposites by DMA at 1 Hz. The neat PCL showed a

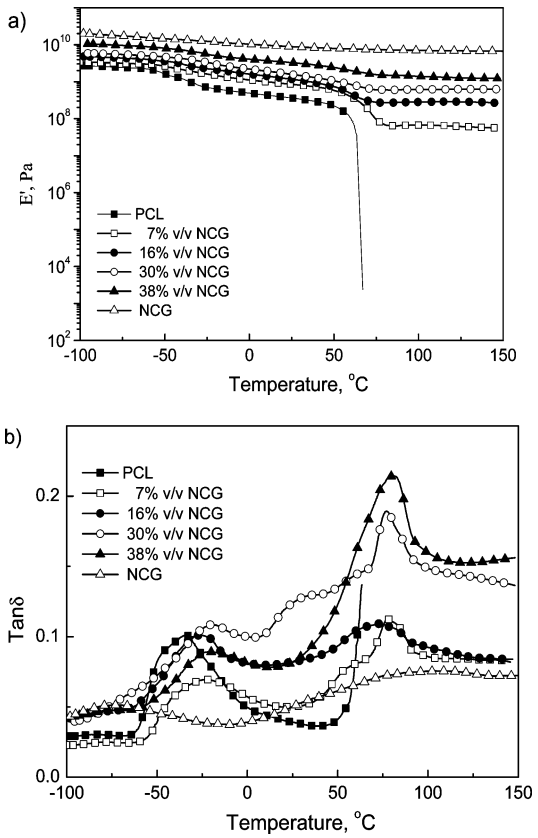

Figure 9. DMA temperature sweeps for NCG/PCL nanocompoites. (a) Storage modulus E' and (b) loss tangent tan δ of nanocomposites as a function of NCG content and temperature.

typical behavior of semi-crystalline polymer. At below −60°C, the neat PCL is in glassy state, with E' nearly constant because of restricted molecular motions.[8] A small decrease in E' between −60 °C and −20 °C is glass transition of amorphous regions of the PCL.[44,56] The melting at 60 °C cause sudden drop of E' to null, resulting from the melting of the crystalline regions of the PCL. Incorporation of cellulose network changes the behavior drastically. While the increase in E' by NCG is modest at below T_g, it becomes significant at above ca. −25°C; finally, collapse by melting is totally suppressed. Similar reinforcement effects on the polymers above T_m have also been reported in 2,2,6,6-tetramehylpiperidine-1-oxyl radical (TEMPO) -oxidized cellulose nanofibers-polystyrene nanocomposites[6] and nanofibrillated cellulose-*g*-PCL nanocomposites.[26] However, E' values of the NCG/PCL nanocomposites are much higher than those of the cellulose nanofibers/nanowhiskers-based PCL nanocomposites at comparable composition,[26,45,56] most probably because of the interconnected nanofibrillar network structure of the NCG was formed by strong intermolecular hydrogen bonding and entanglement of cellulose nanofibers.[60]

From the maximum in loss tangent (tan δ) (Figure 9b), the neat PCL has α-relaxation temperature (T_α) around −37°C. The introduction of NCG into PCL matrix increased T_α to around −21°C with increasing of NCG content. Moreover, the intensity of tan δ peak at around 79°C of the nanocomposites, which cannot be observed in the neat PCL, decreased more than proportionally the NCG content. Considering the different polar nature of cellulose and PCL, a weak hydrogen bonding or van der Waals forces between the PCL matrix and NCG can be expected. Thus, these tendencies are attributed to the substantial restrained mobility of chain segment of PCL due to the strong confinement effects from the interconnected nanofibrillar network structure of the NCG.

Figure 10 show the NCG-content dependence of modulus of nanocomposites at −80, −20, and 100 °C, i.e., below T_g,

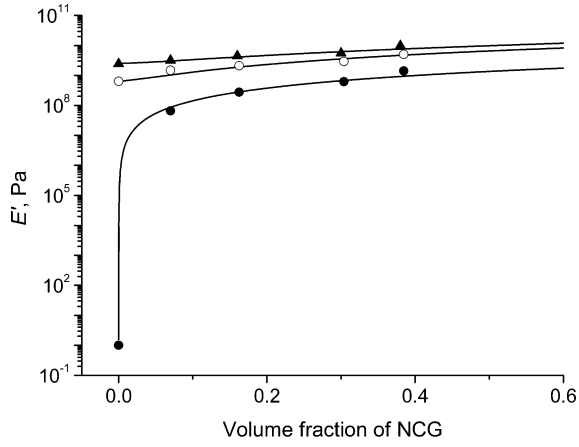

Figure 10. Storage moduli E' of PCL and NCG/PCL nanocomposites at −80°C (▲), −20°C (○), and 100°C (●). Lines show the predictions by the percolation model.

between T_g and T_m, and above T_m of the PCL. The presence of NCG with only 7% v/v enhanced E' by 1.3 times, 10 times, and 8 orders of magnitude from those of the neat PCL at −80, −20, and 100 °C, respectively, demonstrating significant improvement in E' above T_g and T_m of PCL. Dependence of elastic modulus on cellulose content has been studied numerously for cellulose nanofiber/nanowhisker-based nanocomposites, with interpretation by the percolation model giving E' of the nanocomposites as[6,9,21−23]

$$E' = \frac{(1 - 2\psi + \psi X_r)E_s'E_r' + (1 - X_r)\psi E_r'^2}{(1 - X_r)E_r' + (X_r - \psi)E_s'} \quad (6)$$

with

$$\psi = X_r\left(\frac{X_r - X_c}{1 - X_c}\right)^{0.4} \quad (7)$$

and

$$X_c = \frac{0.7}{f} \quad (8)$$

where E_s' = E' of neat polymer; E_r' = E' of percolating cellulosic network; X_r = volume fraction of nanofibers/nanowhiskers; X_c = volume fraction of nanofibers/nanowhiskers at percolation threshold; Ψ = volume fraction of nanofibers/nanowhiskers contributing to percolation ("effective skeleton"); and f = aspect ratio of nanofibers/nanowhiskers.

Because the NCG is intrinsically percolated as long as it is a "gel", X_c must be set zero, making eq 8 irrelevant. Equation 7 is

dx.doi.org/10.1021/am500337p | ACS Appl. Mater. Interfaces 2014, 6, 7204−7213

Table 3. E_r' Values of Cellulose Nanofibers/Nanowhiskers and NCG in Various Polymer Nanocomposites for Percolation Model Simulation

filler	polymer matrix[a]	aspect ratio	T_g/T_α (°C)	E_r', GPa			ref
				$T < T_g$	$T_g < T < T_m$	$T > T_m$	
tunicate nanowhiskers	PHO	67	0		15		61
	EO-EPI	84	−37		4		21, 22
	SBR	84	−46		4		24
	PBD	84	−102		4		22, 24
	PVAc	84	42		4		21
	PS	84	102		4		22
	epoxy	84	170		24		64
	PVA	83	71		80		63
	latex	100	0		5		62
cotton nanowhiskers	PVA	10	71		10		63
	epoxy	11	170		4		64
	EO-EPI	11	−37		0.25		22, 23
	PVA	11	40		10		66
	PLA	16	60		22.8		65
sisal nanowhiskers	PEO	43	−55		8.5		67
wheat straw nanowhiskers	latex	45	0		6		68
TEMPO-oxidized nanofibers	PS	310	102		10		6
nanoporous cellulose gels	PCL	∞	−37	21	16	3.6	this work

[a]PHO, poly(β-hydroxyoctanoate); EO-EPI, ethylene oxide-epichlorohydrin copolymer; SBR, poly(styrene-*co*-butadiene); PBD, polybutadiene; PVAc, poly(vinyl acetate); PS, polystyrene; PVA, Poly(vinyl alcohol); PLA, polylactide; PEO, poly(oxyethylene); PCL, poly(ε-caprolactone); TEMPO, 2,2,6,6-tetramethylpiperidine-1-oxyl.

based on the assumption that elastic modulus is proportional to percolation probability, i.e., fraction of fibrous elements belonging to spanning clusters, or "effective skeleton". Here again, use of this formula to gel is questionable because all elements of a gel belongs to an infinite network. Still, the E' values for NCG/PCL nanocomposites agree well with the percolation model by using experimental values for X_r and E_s' (2.44 GPa at -80°C, 641 MPa at −20°C and less than 1 Pa at 100 °C, respectively, for neat PCL), and fitting values from the experimental data for E_r' (21 GPa at −80°C, 16 GPa at −20 °C, and 3.6 GPa at 100 °C, respectively, for the percolating NCG network), confirming again that the three-dimensional NCG indeed form a percolating network and preserved well in the nanocomposites.

Notably, the predicted E_r' of the NCG for percolating simulation are significantly different with the experimentally determined E' of the NCG film (18.1, 11.8, and 7.0 GPa, respectively, at −80, −20, and 100 °C), and different with the E_r' of tunicate nanowhiskers (4 to 80 GPa),[21,22,24,61−64] cotton nanowhiskers (0.25 to 22.8 GPa),[22,23,63−66] sisal nanowhiskers (8.5 GPa),[67] wheat straw nanowhiskers (6 GPa),[68] and TEMPO-oxidized cellulose nanofibers (10 GPa)[6] for various cellulose nanofiber/nanowhisker−polymer composites (Table 3). Possible causes of this behavior are (i) nanofiller−nanofiller interactions in polymer nanocomposites are strongly depending on type and architecture of cellulosic network, polarity, and T_g of polymer matrix, (ii) difference in the mechanical properties of the NCG film and the percolating NCG network in nanocomposites, (iii) possible changes in the intermolecular hydrogen bonding of cellulose nanofibers and aggregate structure of polymer matrix with temperature. Nevertheless, the agreement with calculation for reinforcement simulation is even better than those for cellulose nanofibers/nanowhikers-based nanocomposites to which percolation model seems to be appropriate at high volume fraction of cellulose. The scaling law formula of eq 7 may be used as a phenomenological description of the gel-type nanocomposites.

Typical stress−strain curves at 25°C clearly show the influence of the NCG on the mechanical behavior of the NCG/PCL nanocomposites (Figure 11). The neat PCL is a ductile semi-crystalline polymer and undergoes large deformation before break in rubbery state, while all nanocomposites exhibit an elastic nonlinear behavior. As expected, the nanocomposites show improved Young's modulus (E) in the presence of NCG (Table 1). However, the elongation at break (ε_b) was reduced from 650% for the neat PCL to around 12% for the nanocomposites regardless NCG content. Moreover, the tensile strength (σ_b) increased gradually from 11 MPa for the neat PCL (stress at break) to 25.8 MPa for the nanocomposites containing 38% v/v NCG, respectively.

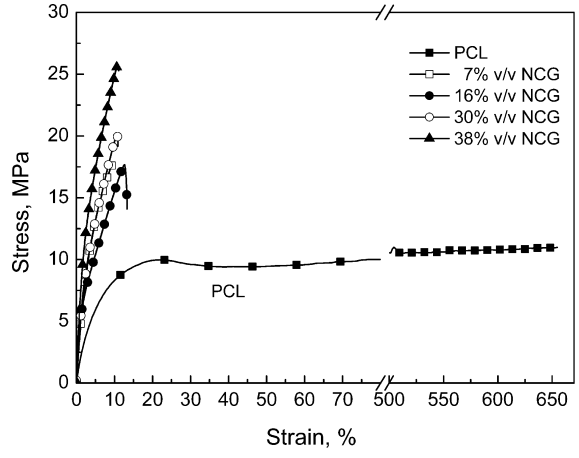

Figure 11. Stress−strain curves of PCL and NCG/PCL nanocomposites containing various NCG content at 25°C.

We examined thermal decomposition of the NCG/PCL nanocomposites by TGA under nitrogen as shown in Figure 12.

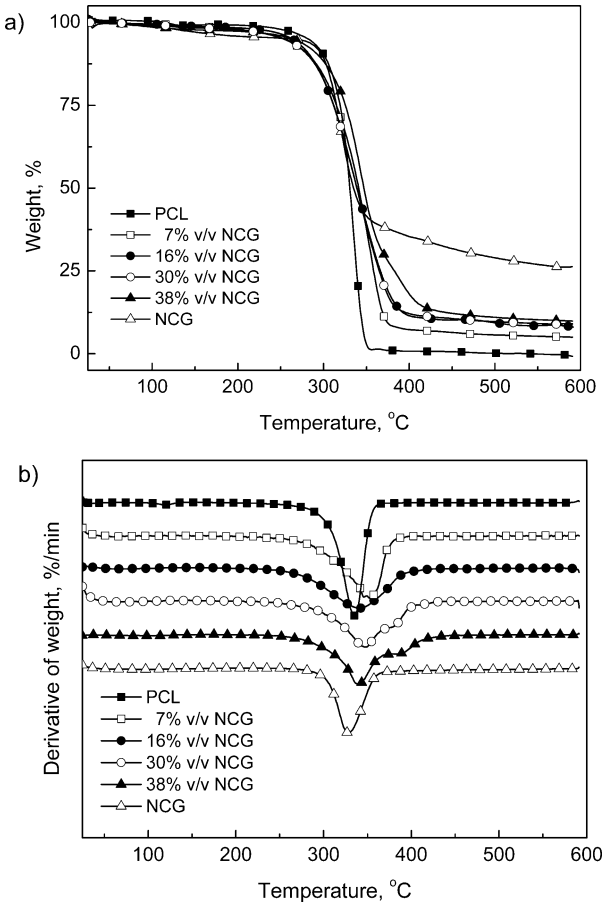

Figure 12. Thermogravimetry analysis (TGA) (a) and derivative thermogravimetry (DTG) (b) curves of NCG, PCL and NCG/PCL nanocomposites containing various NCG content under nitrogen atmosphere.

Although thermal decomposition of cellulose nanowhiskers takes place at less than 150 °C because of the presence of sulfate groups,[37] the NCG withstood heating up to 290–370°C, the decomposition temperature of pristine cellulose. In addition, the hybridization of PCL with NCG resulted in mutual stabilizing effect as seen in the upward shift of DTG peaks from those of neat PCL and NCG (Figure 12b). This behavior is another demonstration of effectiveness of the current approach of NCG-based hybridization of synthetic resins.

CONCLUSIONS

This study has developed a facile route to prepare NCG/PCL nanocomposites by in situ ring-opening polymerization of ε-CL monomer in the nanoporous regenerated cellulose gel from aqueous alkali hydroxide-urea solution. The NCG content of the nanocomposite could be controlled widely, 7–38% v/v, by changing water content of starting hydrogel by compression dewatering. The molecular weight and crystallization of PCL in the nanocomposites were significantly affected by the presence of NCG network. The interconnected nanofibrillar network structure of the NCG were finely distributed and preserved well in PCL matrix. The NCG/PCL nanocomposites showed remarkable improvement in tensile storage modulus above glass transition and melting temperature of PCL, and matched well with the percolation model. This approach of cellulose–synthetic polymer hybridization seems worth further exploration in developing advanced materials for both bulk and high-value-added applications.

ASSOCIATED CONTENT

Supporting Information

Movie S1 demonstrating excellent mechanical stability of the NCG/PCL nanocomposites above the melting temperature of PCL. This material is available free of charge via the Internet at http://pubs.acs.org.

AUTHOR INFORMATION

Corresponding Author

*E-mail: caijie@whu.edu.cn or jiecaiwhu@hotmail.com. Tel: +86-27-8721-6311. Fax: +86-27-6875-4067.

Notes

The authors declare no competing financial interest.

ACKNOWLEDGMENTS

This work was supported by the National Basic Research Program of China (2010CB732203), the National Natural Science Foundation of China (51373125, 20904043, 51273067), and the State Key Program of National Natural Science of China (21334005).

REFERENCES

(1) Darder, M.; Aranda, P.; Ruiz-Hitzky, E. Bionanocomposites: A New Concept of Ecological, Bioinspired, and Functional Hybrid Materials. *Adv. Mater.* **2007**, *19*, 1309–1319.

(2) Reddy, M. M.; Vivekanandhan, S.; Misra, M.; Bhatia, S. K.; Mohanty, A. K. Biobased Plastics and Bionanocomposites: Current Status and Future Opportunities. *Prog. Polym. Sci.* **2013**, *38*, 1653–1689.

(3) Woodruff, M. A.; Hutmacher, D. W. The Return of a Forgotten Polymer-Polycaprolactone in the 21st Century. *Prog. Polym. Sci.* **2010**, *35*, 1217–1256.

(4) Ci, L.; Suhr, J.; Pushparaj, V.; Zhang, X.; Ajayan, P. M. Continuous Carbon Nanotube Reinforced Composites. *Nano Lett.* **2008**, *8*, 2762–2766.

(5) Kaiser, A. B.; Skakalova, V. Electronic Conduction in Polymers, Carbon Nanotubes and Graphene. *Chem. Soc. Rev.* **2011**, *40*, 3786–3801.

(6) Fujisawa, S.; Ikeuchi, T.; Takeuchi, M.; Saito, T.; Isogai, A. Superior Reinforcement Effect of TEMPO-Oxidized Cellulose Nanofibrils in Polystyrene Matrix: Optical, Thermal, and Mechanical Studies. *Biomacromolecules* **2012**, *13*, 2188–2194.

(7) Fujisawa, S.; Saito, T.; Kimura, S.; Iwata, T.; Isogai, A. Surface Engineering of Ultrafine Cellulose Nanofibrils toward Polymer Nanocomposite Materials. *Biomacromolecules* **2013**, *14*, 1541–1546.

(8) Cao, X.; Habibi, Y.; Lucia, L. A. One-pot Polymerization, Surface Grafting, and Processing of Waterborne Polyurethane-Cellulose Nanocrystal Nanocomposites. *J. Mater. Chem.* **2009**, *19*, 7137–7145.

(9) Siqueira, G.; Bras, J.; Dufresne, A. Cellulose Whiskers versus Microfibrils: Influence of the Nature of the Nanoparticle and its Surface Functionalization on the Thermal and Mechanical Properties of Nanocomposites. *Biomacromolecules* **2009**, *10*, 425–432.

(10) Habibi, Y.; Lucia, L. A.; Rojas, O. J. Cellulose Nanocrystals: Chemistry, Self-Assembly, and Applications. *Chem. Rev.* **2010**, *110*, 3479–3500.

(11) Shopsowitz, K. E.; Qi, H.; Hamad, W. Y.; MacLachlan, M. J. Free-standing Mesoporous Silica Films with Tunable Chiral Nematic Structures. *Nature* **2010**, *468*, 422–425.

(12) Kelly, J. A.; Shopsowitz, K. E.; Ahn, J. M.; Hamad, W. Y.; MacLachlan, M. J. Chiral Nematic Stained Glass: Controlling the

Optical Properties of Nanocrystalline Cellulose-Templated Materials. *Langmuir* **2012**, *28*, 17256−17262.
(13) Xu, Q.; Kong, Q.; Liu, Z.; Wang, X.; Liu, R.; Zhang, J.; Yue, L.; Duan, Y.; Cui, G. Cellulose/Polysulfonamide Composite Membrane as High Performance Lithium-ion Battery Separator. *ACS Sustainable Chem. Eng.* **2014**, *2*, 194−199.
(14) Xu, X.; Liu, F.; Jiang, L.; Zhu, J. Y.; Haagenson, D.; Wiesenborn, D. P. Cellulose Nanocrystals vs. Cellulose Nanofibrils: A Comparative Study on Their Microstructures and Effects as Polymer Reinforcing Agents. *ACS Appl. Mater. Interfaces* **2013**, *5*, 2999−3009.
(15) Bitinis, N.; Hernandez, M.; Verdejo, R.; Kenny, J. M.; Lopez-Manchado, M. A. Recent Advances in Clay/Polymer Nanocomposites. *Adv. Mater.* **2011**, *23*, 5229−5236.
(16) Kiliaris, P.; Papaspyrides, C. D. Polymer/Layered Silicate (Clay) Nanocomposites: An Overview of Flame Retardancy. *Prog. Polym. Sci.* **2010**, *35*, 902−958.
(17) Hu, K. S.; Gupta, M. K.; Kulkarni, D. D.; Tsukruk, V. V. Ultra-Robust Graphene Oxide-Silk Fibroin Nanocomposite Membranes. *Adv. Mater.* **2013**, *25*, 2301−2307.
(18) Kim, H.; Abdala, A. A.; Macosko, C. W. Graphene/Polymer Nanocomposites. *Macromolecules* **2010**, *43*, 6515−6530.
(19) Veedu, V. P.; Cao, A.; Li, X.; Ma, K.; Soldano, C.; Kar, S.; Ajayan, P. M.; Ghasemi-Nejhad, M. N. Multifunctional Composites using Reinforced Laminae with Carbon-Nanotube Forests. *Nat. Mater.* **2006**, *5*, 457−462.
(20) Nardecchia, S.; Carriazo, D.; Ferrer, M. L.; Gutierrez, M. C.; del Monte, F. Three Dimensional Macroporous Architectures and Aerogels Built of Carbon Nanotubes and/or Graphene: Synthesis and Applications. *Chem. Soc. Rev.* **2013**, *42*, 794−830.
(21) Capadona, J. R.; Shanmuganathan, K.; Tyler, D. J.; Rowan, S. J.; Weder, C. Stimuli-Responsive Polymer Nanocomposites Inspired by the Sea Cucumber Dermis. *Science* **2008**, *319*, 1370−1374.
(22) Capadona, J.; Van Den Berg, O.; Capadona, L.; Schroeter, M.; Rowan, S.; Tyler, D.; Weder, C. A Versatile Approach for the Processing of Polymer Nanocomposites with Self-assembled Nanofibre Templates. *Nat. Nanotechnol.* **2007**, *2*, 765−769.
(23) Capadona, J. R.; Shanmuganathan, K.; Trittschuh, S.; Seidel, S.; Rowan, S. J.; Weder, C. Polymer Nanocomposites with Nanowhiskers Isolated from Microcrystalline Cellulose. *Biomacromolecules* **2009**, *10*, 712−716.
(24) Dagnon, K. L.; Shanmuganathan, K.; Weder, C.; Rowan, S. J. Water-Triggered Modulus Changes of Cellulose Nanofiber Nanocomposites with Hydrophobic Polymer Matrices. *Macromolecules* **2012**, *45*, 4707−4715.
(25) Mendez, J.; Annamalai, P. K.; Eichhorn, S. J.; Rusli, R.; Rowan, S. J.; Foster, E. J.; Weder, C. Bioinspired Mechanically Adaptive Polymer Nanocomposites with Water-Activated Shape-Memory Effect. *Macromolecules* **2011**, *44*, 6827−6835.
(26) Boujemaoui, A.; Carlsson, L.; Malmström, E.; Lahcini, M.; Berglund, L.; Sehaqui, H.; Carlmark, A. Facile Preparation Route for Nanostructured Composites: Surface-Initiated Ring-Opening Polymerization of ε-Caprolactone from High-Surface-Area Nanopaper. *ACS Appl. Mater. Interfaces* **2012**, *4*, 3191−3198.
(27) Quero, F.; Eichhorn, S. J.; Nogi, M.; Yano, H.; Lee, K. Y.; Bismarck, A. Interfaces in Cross-Linked and Grafted Bacterial Cellulose/Poly(Lactic Acid) Resin Composites. *J. Polym. Environ.* **2012**, *20*, 916−925.
(28) Nogi, M.; Yano, H. Transparent Nanocomposites Based on Cellulose Produced by Bacteria Offer Potential Innovation in the Electronics Device Industry. *Adv. Mater.* **2008**, *20*, 1849−1852.
(29) Ifuku, S.; Nogi, M.; Abe, K.; Handa, K.; Nakatsubo, F.; Yano, H. Surface Modification of Bacterial Cellulose Nanofibers for Property Enhancement of Optically Transparent Composites: Dependence on Acetyl-group DS. *Biomacromolecules* **2007**, *8*, 1973−1978.
(30) Klemm, D.; Kramer, F.; Moritz, S.; Lindström, T.; Ankerfors, M.; Gray, D.; Dorris, A. Nanocelluloses: A New Family of Nature-Based Materials. *Angew. Chem., Int. Ed.* **2011**, *50*, 5438−5466.
(31) Eichhorn, S. J. Stiff as a Board: Perspectives on the Crystalline Modulus of Cellulose. *ACS Macro Lett.* **2012**, *1*, 1237−1239.
(32) Moon, R. J.; Martini, A.; Nairn, J.; Simonsen, J.; Youngblood, J. Cellulose Nanomaterials Review: Structure, Properties and Nanocomposites. *Chem. Soc. Rev.* **2011**, *40*, 3941−3994.
(33) Beecher, J. F. Wood, Trees and Nanotechnology. *Nat. Nanotechnol.* **2007**, *2*, 466−467.
(34) Eichhorn, S. J.; Dufresne, A.; Aranguren, M.; Marcovich, N. E.; Capadona, J. R.; Rowan, S. J.; Weder, C.; Thielemans, W.; Roman, M.; Renneckar, S.; Gindl, W.; Veigel, S.; Keckes, J.; Yano, H.; Abe, K.; Nogi, M.; Nakagaito, A. N.; Mangalam, A.; Simonsen, J.; Benight, A. S.; Bismarck, A.; Berglund, L. A.; Peijs, T. Review: Current International Research into Cellulose Nanofibres and Nanocomposites. *J. Mater. Sci.* **2010**, *45*, 1−33.
(35) Zhou, C.; Shi, Q.; Guo, W.; Terrell, L.; Qureshi, A. T.; Hayes, D. J.; Wu, Q. Electrospun Bio-Nanocomposite Scaffolds for Bone Tissue Engineering by Cellulose Nanocrystals Reinforcing Maleic Anhydride Grafted PLA. *ACS Appl. Mater. Interfaces* **2013**, *5*, 3847−3854.
(36) Yang, X.; Bakaic, E.; Hoare, T.; Cranston, E. D. Injectable Polysaccharide Hydrogels Reinforced with Cellulose Nanocrystals: Morphology, Rheology, Degradation, and Cytotoxicity. *Biomacromolecules* **2013**, *14*, 4447−4455.
(37) Lin, N.; Dufresne, A. Physical and/or Chemical Compatibilization of Extruded Cellulose Nanocrystal Reinforced Polystyrene Nanocomposites. *Macromolecules* **2013**, *46*, 5570−5583.
(38) Rosilo, H.; Kontturi, E.; Seitsonen, J.; Kolehmainen, E.; Ikkala, O. Transition to Reinforced State by Percolating Domains of Intercalated Brush-Modified Cellulose Nanocrystals and Poly(butadiene) in Cross-Linked Composites Based on Thiol−ene Click Chemistry. *Biomacromolecules* **2013**, *14*, 1547−1554.
(39) Brown, E. E.; Hu, D.; Abu Lail, N.; Zhang, X. Potential of Nanocrystalline Cellulose−Fibrin Nanocomposites for Artificial Vascular Graft Applications. *Biomacromolecules* **2013**, *14*, 1063−1071.
(40) Goffin, A.-L.; Habibi, Y.; Raquez, J.-M.; Dubois, P. Polyester-Grafted Cellulose Nanowhiskers: A New Approach for Tuning the Microstructure of Immiscible Polyester Blends. *ACS Appl. Mater. Interfaces* **2012**, *4*, 3364−3371.
(41) Khoshkava, V.; Kamal, M. R. Effect of Surface Energy on Dispersion and Mechanical Properties of Polymer/Nanocrystalline Cellulose Nanocomposites. *Biomacromolecules* **2013**, *14*, 3155−3163.
(42) Lönnberg, H.; Fogelström, L.; Berglund, L.; Malmström, E.; Hult, A. Surface grafting of microfibrillated cellulose with poly(ε-caprolactone) − Synthesis and characterization. *Eur. Polym. J.* **2008**, *44*, 2991−2997.
(43) Lönnberg, H.; Larsson, K.; Lindström, T.; Hult, A.; Malmström, E. Synthesis of Polycaprolactone-Grafted Microfibrillated Cellulose for Use in Novel Bionanocomposites−Influence of the Graft Length on the Mechanical Properties. *ACS Appl. Mater. Interfaces* **2011**, *3*, 1426−1433.
(44) Lönnberg, H.; Zhou, Q.; Brumer, H.; Teeri, T. T.; Malmström, E.; Hult, A. Grafting of Cellulose Fibers with Poly(ε-caprolactone) and Poly(L-lactic acid) via Ring-Opening Polymerization. *Biomacromolecules* **2006**, *7*, 2178−2185.
(45) Zoppe, J. O.; Peresin, M. S.; Habibi, Y.; Venditti, R. A.; Rojas, O. J. Reinforcing Poly(ε-caprolactone) Nanofibers with Cellulose Nanocrystals. *ACS Appl. Mater. Interfaces* **2009**, *1*, 1996−2004.
(46) Cai, J.; Zhang, L. Rapid Dissolution of Cellulose in LiOH/Urea and NaOH/Urea Aqueous Solutions. *Macromol. Biosci.* **2005**, *5*, 539−548.
(47) Cai, J.; Kimura, S.; Wada, M.; Kuga, S.; Zhang, L. Cellulose Aerogels from Aqueous Alkali Hydroxide-Urea Solution. *ChemSusChem* **2008**, *1*, 149−154.
(48) Cai, J.; Kimura, S.; Wada, M.; Kuga, S. Nanoporous Cellulose as Metal Nanoparticles Support. *Biomacromolecules* **2008**, *10*, 87−94.
(49) Cai, J.; Liu, S.; Feng, J.; Kimura, S.; Wada, M.; Kuga, S.; Zhang, L. Cellulose−Silica Nanocomposite Aerogels by In-Situ Formation of Silica in Cellulose Gel. *Angew. Chem., Int. Ed.* **2012**, *124*, 2118−2121.
(50) Shi, Z.; Gao, H.; Feng, J.; Ding, B.; Cao, X.; Kuga, S.; Wang, Y.; Zhang, L.; Cai, J. In situ Synthesis of Robust Conductive Cellulose/Polypyrrole Composite Aerogels and Their Potential Application in

Nerve Regeneration. *Angew. Chem., Int. Ed.* **2014**, DOI: 10.1002/anie.201402751.
(51) Wang, Q. Y.; Cai, J.; Zhang, L. N.; Xu, M.; Cheng, H.; Han, C. C.; Kuga, S.; Xiao, J.; Xiao, R. A Bioplastic with High Strength Constructed from a Cellulose Hydrogel by Changing the Aggregated Structure. *J. Mater. Chem. A* **2013**, *1*, 6678−6686.
(52) Hayashi, T.; Nakayama, K.; Mochizuki, M.; Masuda, T. Studies on biodegradable poly(hexano-6-lactone) fibers. Part 3. Enzymatic degradation in vitro - (IUPAC technical report). *Pure Appl. Chem.* **2002**, *74*, 869−880.
(53) Janata, M.; Masař, B.; Toman, L.; Vlček, P.; Látalová, P.; Brus, J.; Holler, P. Synthesis of Novel Types of Graft Copolymers by a "Grafting-from" Method using Ring-opening Polymerization of Lactones and Lactides. *React. Funct. Polym.* **2003**, *57*, 137−146.
(54) Shu, J.; Chen, Q.; Zhang, S. M. Quantification of Cross Polarization with Relaxation Compensated Reciprocity Relation in NMR. *Chem. Phys. Lett.* **2008**, *462*, 125−128.
(55) Zhao, H.; Shu, J.; Chen, Q.; Zhang, S. Quantitative Structural Characterization of POSS and Octavinyl-POSS Nanocomposites by Solid State NMR. *Solid State Nucl. Magn. Reson.* **2012**, *43-44*, 56−61.
(56) Habibi, Y.; Goffin, A.-L.; Schiltz, N.; Duquesne, E.; Dubois, P.; Dufresne, A. Bionanocomposites Based on Poly(ε-caprolactone)-grafted Cellulose Nanocrystals by Ring-opening Polymerization. *J. Mater. Chem.* **2008**, *18*, 5002−5010.
(57) Cai, J.; Zhang, L.; Zhou, J.; Qi, H.; Chen, H.; Kondo, T.; Chen, X.; Chu, B. Multifilament Fibers Based on Dissolution of Cellulose in NaOH/Urea Aqueous Solution: Structure and Properties. *Adv. Mater.* **2007**, *19*, 821−825.
(58) Wang, J.; Cheung, M. K.; Mi, Y. Miscibility and Morphology in Crystalline/Amorphous Blends of Poly(caprolactone)/Poly(4-vinylphenol) as Studied by DSC, FTIR, and ^{13}C Solid State NMR. *Polymer* **2002**, *43*, 1357−1364.
(59) Xiao, L.; Mai, Y.; He, F.; Yu, L.; Zhang, L.; Tang, H.; Yang, G. Bio-based Green Composites with High Performance from Poly(lactic acid) and Surface-modified Microcrystalline Cellulose. *J. Mater. Chem.* **2012**, *22*, 15732−15739.
(60) Cai, J.; Zhang, L. Unique Gelation Behavior of Cellulose in NaOH/Urea Aqueous Solution. *Biomacromolecules* **2006**, *7*, 183−189.
(61) Dubief, D.; Samain, E.; Dufresne, A. Polysaccharide Microcrystals Reinforced Amorphous Poly(β-hydroxyoctanoate) Nanocomposite Materials. *Macromolecules* **1999**, *32*, 5765−5771.
(62) Favier, V.; Cavaille, J. Y.; Canova, G. R.; Shrivastava, S. C. Mechanical Percolation in Cellulose Whisker Nanocomposites. *Polym. Eng. Sci.* **1997**, *37*, 1732−1739.
(63) Jorfi, M.; Roberts, M. N.; Foster, E. J.; Weder, C. Physiologically Responsive, Mechanically Adaptive Bio-Nanocomposites for Biomedical Applications. *ACS Appl. Mater. Interfaces* **2013**, *5*, 1517−1526.
(64) Tang, L.; Weder, C. Cellulose Whisker/Epoxy Resin Nanocomposites. *ACS Appl. Mater. Interfaces* **2010**, *2*, 1073−1080.
(65) Braun, B.; Dorgan, J. R.; Hollingsworth, L. O. Supra-Molecular EcoBioNanocomposites Based on Polylactide and Cellulosic Nanowhiskers: Synthesis and Properties. *Biomacromolecules* **2012**, *13*, 2013−2019.
(66) Roohani, M.; Habibi, Y.; Belgacem, N. M.; Ebrahim, G.; Karimi, A. N.; Dufresne, A. Cellulose Whiskers Reinforced Polyvinyl Alcohol Copolymers Nanocomposites. *Eur. Polym. J.* **2008**, *44*, 2489−2498.
(67) Alloin, F.; D'Aprea, A.; Kissi, N. E.; Dufresne, A.; Bossard, F. Nanocomposite Polymer Electrolyte Based on Whisker or Microfibrils Polyoxyethylene Nanocomposites. *Electrochim. Acta* **2010**, *55*, 5186−5194.
(68) Dufresne, A.; Cavaillé, J.-Y.; Helbert, W. Thermoplastic Nanocomposites Filled with Wheat Straw Cellulose Whiskers. Part II: Effect of Processing and Modeling. *Polym. Compos.* **1997**, *18*, 198−210.